AENSI Journals

Australian Journal of Basic and Applied Sciences

ISSN:1991-8178

Journal home page: www.ajbasweb.com

Performance and Measurement of Current Control Schemes in Grid connected Inverters

[1]T. Yuvaraja and [2]M. Gopinath

[1]*Meenakshi Academy of Higher Education & Research, Department of Electrical and Electronics ,Research Scholar, Chennai City, India.*
[2]*Dr. NGP Institute of Technology, Department of Electrical and Electronics, Professor, Coimbatore City, India*

ARTICLE INFO

Article history:
Received 2 March 2014
Received in revised form
13 May 2014
Accepted 28 May 2014
Available online 23 June 2014

Keywords:
PIR, PWM

ABSTRACT

Background: Applications such as digital based control in grid connected output currents are measured accurately. So obtaining the accuracy I must in the design consideration. The proposed work analyze the single and three phase measurement of grid connected inverter and the current control strategy is viewed.

To Cite This Article: T. Yuvaraja, M. Gopinath, Performance and Measurement of Current Control Schemes in Grid connected Inverters. ***Aust. J. Basic & Appl. Sci.,*** *8(9): 163-170, 2014*

INTRODUCTION

Single-phase Grid-connected Inverters:

Fig. 1 presents the block diagram of the current control in consideration of the measurement offsets of the utility voltage and output current in single-phase grid-connected inverters. In Fig. 1, *δvg* and *δig* denote the measurement offsets in the utility voltage and the inverter output current, respectively, whereas *vgm* and *ig_m* denote the measured utility voltage and inverter output current, respectively. On the assumption that the utility voltage is a complete sinusoidal wave as expressed in Equation (1), the inverter output current reference is expressed as Equation (2) so that active and reactive power may be regulated at the utility side, the pulse width modulation (PWM) is ideal, and the measurement offsets are constant. The inverter output current at the steady state in the current control using a proportional-integral-resonant (PIR) regulator (as expressed in Equation (3)) is expressed in Equation (4).

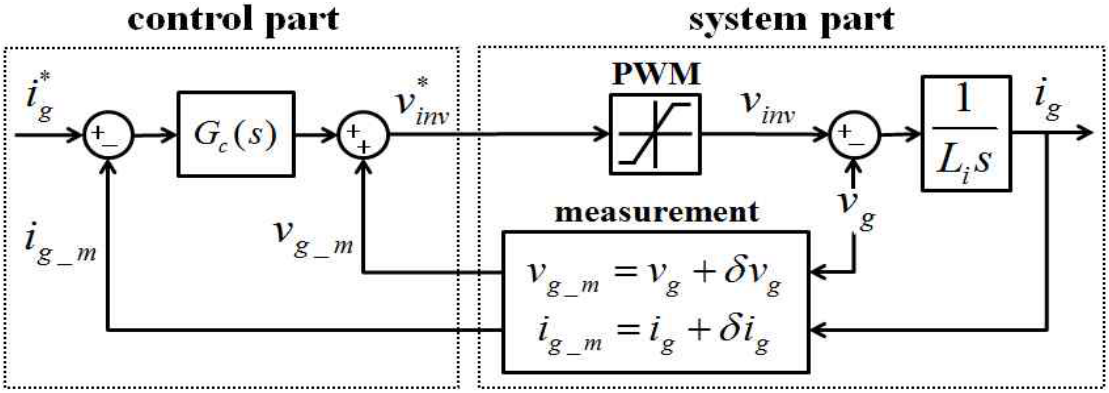

Fig. 1: Block diagram of the current control in measurement in single-phase grid-connected inverters.

$$v_g = V_g \sin \omega t \tag{1}$$

$$i_g^* = I_d^{e*} \sin \omega t + I_q^{e*} \cos \omega t \tag{2}$$

Corresponding Author: T. Yuvaraja, Meenakshi Academy of Higher Education & Research, Department of Electrical and Electronics ,Research Scholar, Chennai City, India.
E-mail: yuvarajastr@gmail.com

$$G_c(s) = K_{pc} + \frac{K_{ic}}{s} + \frac{K_{rc}s}{s^2 + \omega_0^2} \tag{3}$$

$$i_g = I_d^{e*} \sin \omega t + I_q^{e*} \cos \omega t - \delta i_g \tag{4}$$

As Equation (4) shows, the current measurement offset causes the DC current component injected into the utility side in single-phase grid-connected inverters. At the steady state, using Equations (1) and (4) yields the inverter output voltage as follows:

$$\begin{aligned} v_{inv} &= L_i \frac{di_g}{dt} + v_g \\ &= \omega L_i I_d^{e*} \cos \omega t - \omega L_i I_q^{e*} \sin \omega t + V_g \sin \omega t \end{aligned} \tag{5}$$

If no power loss occurs in the inverter, the power supplied from the DC-link to the inverter is similar to the inverter output power and can be expressed as Equation (6).

$$p_{out\_1r} = -P_S \left\{ \delta i_g \sin(\omega t + \phi_S) \right\} \tag{6}$$

If the DC-link capacitor voltage is maintained at the constant operating point (*Vdc**), the power absorbed in the DC-link capacitor can be obtained as follows:

$$\begin{aligned} p_{dc} &= \frac{C_{dc}}{2} \frac{dv_{dc}^2}{dt} \\ &= P_s \left\{ \delta i_g \sin(\omega t + \phi_S) + \frac{I_d^{e*}}{2} \cos(2\omega t + \phi_S) - \frac{I_q^{e*}}{2} \sin(2\omega t + \phi_S) \right\} \end{aligned} \tag{7}$$

Equation (7) shows that the current measurement offset causes the DC-link capacitor voltage to oscillate at the utility voltage frequency in single-phase grid-connected inverters. This ripple deteriorates the overall system performance because it generates inverter output current reference with harmonics; thus, the real inverter output current also has harmonic components.

Three-phase Grid-connected Inverters:

Fig. 3 presents the block diagram of the current control in consideration of the measurement offsets in three-phase grid-connected inverters. In Fig. 3, the stationary dq-axis measurement offsets of utility voltages and inverter output current, respectively, whereas the stationary dq-axis measurement values of utility voltages and inverter output current, respectively. If the utility phase voltages are sinusoidal-balanced voltages, the stationary dq-axis voltages are expressed as Equation (8). The stationary dq-axis reference values of the inverter output phase current can be expressed as Equation (9) to control the active and reactive power at the utility side. Moreover, if the space vector pulse width modulation is ideal and the measurement offsets are constant, the stationary dq-axis output currents at the steady state in the current control system using a PIR regulator are expressed as Equation (10).

$$\begin{aligned} e_d^s &= E \cos \omega t \\ e_q^s &= E \sin \omega t \end{aligned} \tag{8}$$

$$\begin{aligned} i_d^{s*} &= I_d^{e*} \cos \omega t - I_q^{e*} \sin \omega t \\ i_q^{s*} &= I_d^{e*} \sin \omega t + I_q^{e*} \cos \omega t \end{aligned} \tag{9}$$

$$\begin{aligned} i_d^s &= I_d^{e*} \cos \omega t - I_q^{e*} \sin \omega t - \delta i_d^s \\ i_q^s &= I_d^{e*} \sin \omega t + I_q^{e*} \cos \omega t - \delta i_q^s \end{aligned} \tag{10}$$

Equation (10) shows that the current measurement offsets cause DC current components injected into the utility side in three-phase grid-connected inverters. At the steady state, using Equations (8) and (10) yields stationary dq-axis inverter output voltages as follows:

$$v_d^s = L_i \frac{di_d^s}{dt} + e_d^s$$
$$= -\omega L_i I_d^{e*} \sin \omega t - \omega L_i I_q^{e*} \cos \omega t + E \cos \omega t \tag{11}$$

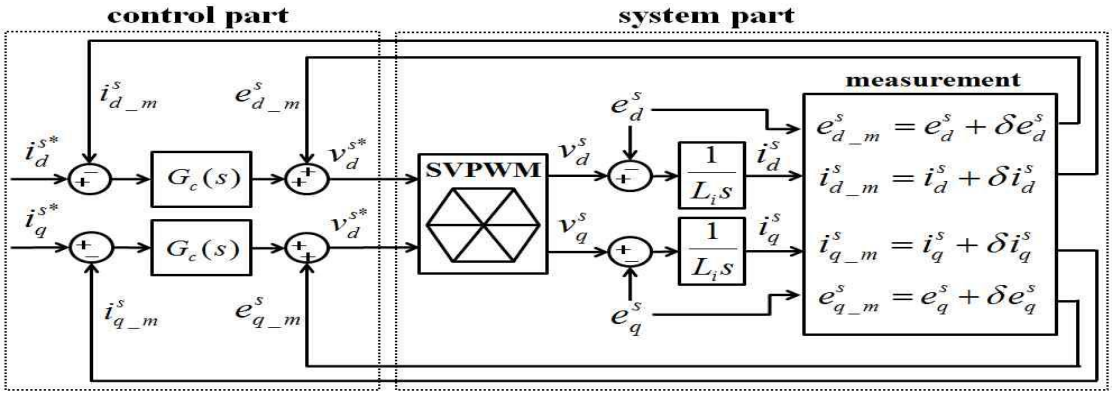

Fig. 3: Block diagram of the current control in measurement of three-phase grid-connected inverters.

If no power loss occurs in the inverter, the power supplied from the DC-link to the inverter is similar to the inverter output power and can be expressed as Equation (12).

$$p_{out\_dc} = \frac{3}{2} E I_d^{e*} \tag{12}$$

If the DC-link capacitor voltage is maintained at the constant operating point (*Vdc**), the power absorbed in the DC-link capacitor can be obtained as follows:

$$p_{dc} = \frac{C_{dc}}{2} \frac{dv_{dc}^2}{dt}$$
$$= \frac{3}{2} P_T \left\{ \delta i_d^s \cos(\omega t + \phi_T) + \delta i_q^s \sin(\omega t + \phi_T) \right\} \tag{13}$$

Equation (13) shows that current measurement offsets cause the DC-link capacitor voltage to oscillate at the utility voltage frequency in three-phase grid-connected inverters. This ripple deteriorates the overall system performance because it generates inverter output current references with harmonics. Thus, real inverter output currents also have harmonic components.

Design Consideration:

Current Measuring Single-phase Grid-connected Inverters:

From Equation (7), the equation for the ripple component of the DC-link capacitor voltage can be calculated as follows:

$$v_{dc\_rip}^2 = v_{dc}^2 - V_{dc}^{*2} = \frac{2}{C_{dc}} \int p_{dc} dt$$
$$= \frac{2P_S}{\omega C_{dc}} \left\{ -\delta i_g \cos(\omega t + \phi_S) \right\}$$
$$+ \frac{2P_S}{\omega C_{dc}} \left\{ \frac{I_d^{e*}}{4} \sin(2\omega t + \phi_S) + \frac{I_q^{e*}}{4} \cos(2\omega t + \phi_S) \right\} \tag{14}$$

Equation (14) can be approximated as Equation (15) because the magnitude of the utility voltage is much larger than the impedance drop

$$v_{dc\_rip}^2 \cong \frac{2V_g}{\omega C_{dc}}\left\{-\delta i_g \cos\omega t + \frac{I_d^{e*}}{4}\sin 2\omega t + \frac{I_q^{e*}}{4}\cos 2\omega t\right\} \tag{15}$$

As shown in Equation (15), the second-order ripple component exists in single-phase grid-connected inverters. The band pass filter expressed in Equation (16) is used to detect the first-order ripple component included in the current measurement offset.

$$T_{BPF}(s) = \frac{BWs}{s^2 + BWs + \omega_{BPF}^2} \tag{16}$$

where *BW* and *ωBPF* are the bandwidth and the center frequency of the band pass filter, respectively. If *ωBPF* is similar to the utility frequency, the first-order ripple component can be obtained with

$$x_q = -\frac{2V_g}{\omega C_{dc}}\delta i_g \cos\omega t\,. \tag{17}$$

The first-order ripple component expressed in Equation (17) is then filtered through the all-pass filter expressed in Equation (18). When *ωAPF* is equal to the utility frequency, the all-pass filter generates a virtual component expressed as Equation (19), which leads the first-order ripple component by 90°.

$$T_{APF}(s) = \frac{s - \omega_{APF}}{s + \omega_{APF}} \tag{18}$$

$$x_d = \frac{2V_g}{\omega C_{dc}}\delta i_g \sin\omega t \tag{19}$$

By substituting Equations (17) and (19) into Equation (20), the magnitude of the first-order ripple component can be established as Equation (21).

$$m = \begin{bmatrix}\sin\omega t & -\cos\omega t\end{bmatrix}\begin{bmatrix}x_d \\ x_q\end{bmatrix} \tag{20}$$

$$m = \frac{2V_g}{\omega C_{dc}}\delta i_g \tag{21}$$

The current measurement offset can be calculated with Equation (21), but the real value cannot be determined without exact parameter values. Moreover, the current measurement offset may be altered by external factors. Hence, a current offset controller is used to maintain the calculated first-order component at zero (Fig. 4). Fig. 5 presents the block diagram of a current control system using the proposed current offset compensator in single-phase grid-connected inverters. The current offset compensator is mainly composed of the first-order ripple component detector, the magnitude detector, and the current offset controller. In Fig. 5, *io_com* is a compensation value for the current measurement offset.

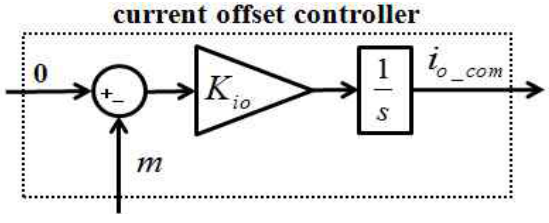

Fig. 4: Block diagram of a current offset controller in single-phase grid-connected inverters.

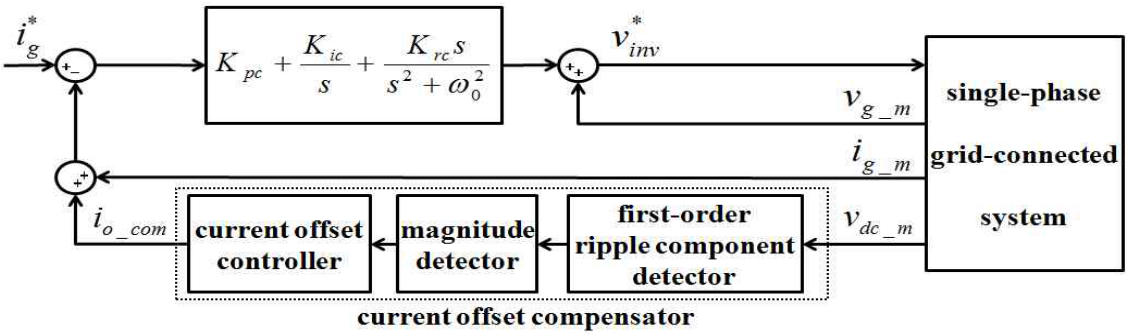

Fig. 5: Block diagram of a current control system using the proposed current offset compensator in single-phase grid-connected inverters.

Current Measuring Three-phase Grid-connected Inverters:

From Equation (13), the equation for the ripple component of the DC-link capacitor voltage can be calculated as follows:

$$v_{dc\_rip}^2 = v_{dc}^2 - V_{dc}^{*2} = \frac{2}{C_{dc}}\int p_{dc}dt$$
$$= \frac{3P_T}{\omega C_{dc}}\left\{\delta i_d^s \sin(\omega t + \phi_T) - \delta i_q^s \cos(\omega t + \phi_T)\right\} \quad (22)$$

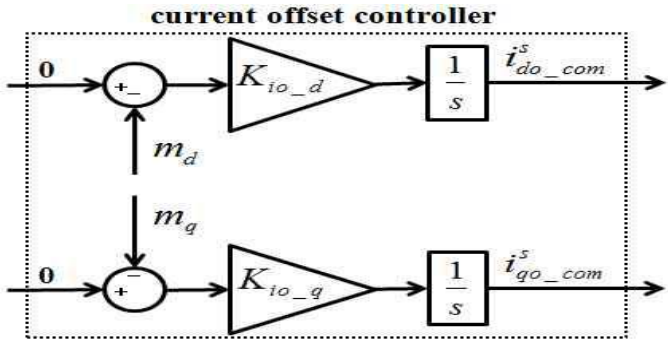

Fig. 6: Block diagram of a current offset controller in three-phase grid-connected inverters.

Equation (22) can be approximated as Equation (23) because the magnitude of the utility voltage is much larger than the impedance drop.

$$x_q \cong \frac{3E}{\omega C_{dc}}\left(\delta i_d^s \sin\omega t - \delta i_q^s \cos\omega t\right) \quad (23)$$

Using the all-pass filter expressed in Equation (18), the virtual component that leads the first-order ripple component by 90° can be obtained as follows:

$$x_d = \frac{3E}{\omega C_{dc}}\left(\delta i_d^s \cos\omega t + \delta i_q^s \sin\omega t\right) \quad (24)$$

The magnitude of the d-axis and q-axis voltage ripple can be obtained with Equation (26) by substituting Equations (23) and (24) into Equation (25).

$$\begin{bmatrix} m_d \\ m_q \end{bmatrix} = \begin{bmatrix} \cos\omega t & \sin\omega t \\ \sin\omega t & -\cos\omega t \end{bmatrix}\begin{bmatrix} x_d \\ x_q \end{bmatrix} \quad (25)$$

$$\begin{bmatrix} m_d \\ m_q \end{bmatrix} = \begin{bmatrix} \frac{3E}{\omega C_{dc}} \delta i_d^s \\ \frac{3E}{\omega C_{dc}} \delta i_q^s \end{bmatrix} \tag{26}$$

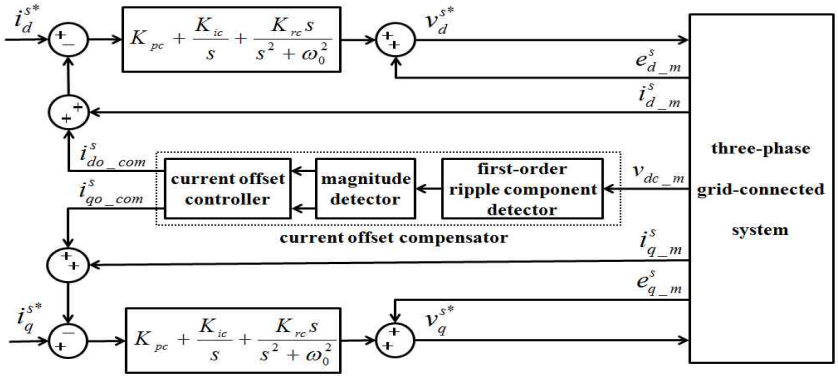

Fig. 7: Block diagram of a current control system using the proposed current offset compensator in three-phase grid-connected inverters.

Similar to single-phase grid-connected inverters, using a current offset controller (Fig. 6) is necessary. Fig. 7 presents the block diagram of a current control system using the proposed current offset compensator in three-phase grid-connected inverters. In Fig 7, stationary dq-axis compensation values for current measurement offsets are represented.

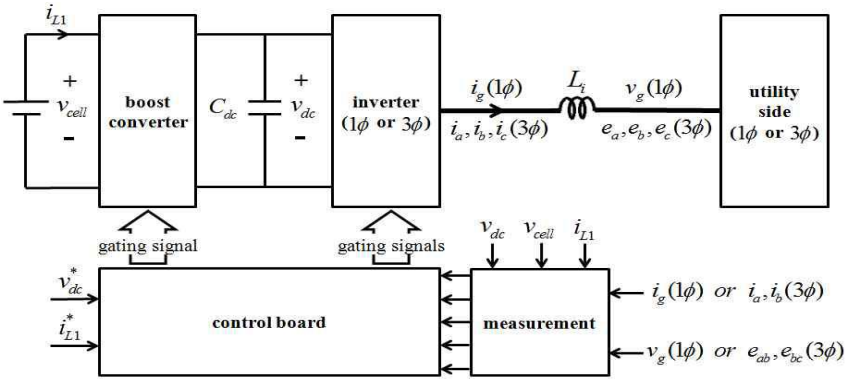

Fig. 8: Sample distributed generation system for simulations and experiments.

Simulation Results:

Simulations and experiments were conducted with a sample distributed generation system (Fig. 8) to investigate

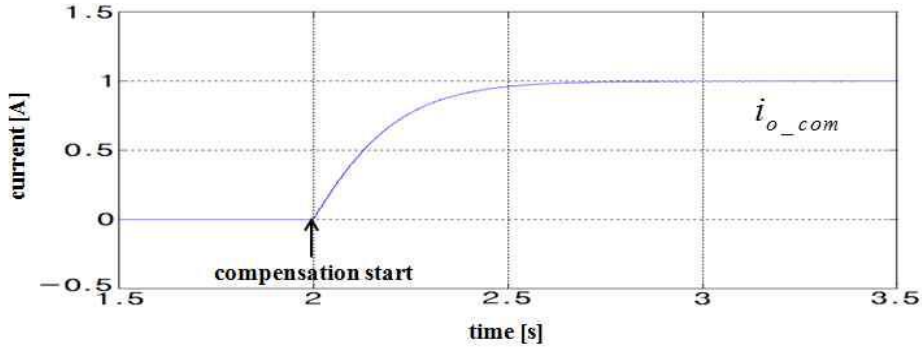

Fig. 9: Output of the current offset compensator in single-phase. grid-connected inverters.

Simulations and experiments were conducted with a sample distributed generation system (Fig. 8) to investigate In the case of single-phase grid-connected inverters; a second-order voltage ripple that distorts the inverter output current inevitably exists in the DC-link capacitor voltage. A notch filter whose centre frequency is twice the utility frequency was utilized to eliminate the effect of the ripple component. Fig. 9 shows an output of the current offset Fig. 9 shows an output of the current offset compensator in single-phase grid-connected inverters. In the figure, the output of the current offset compensator converges at 1 A at the steady state to eliminate the effect of the current measurement offset. Fig. 10 shows the output of the current offset compensator in three-phase grid-connected inverters. Similar to single-phase grid-connected inverters, the current offset compensator calculates the compensation values at the steady state. The effect of the current measurement offset is thus eliminated.

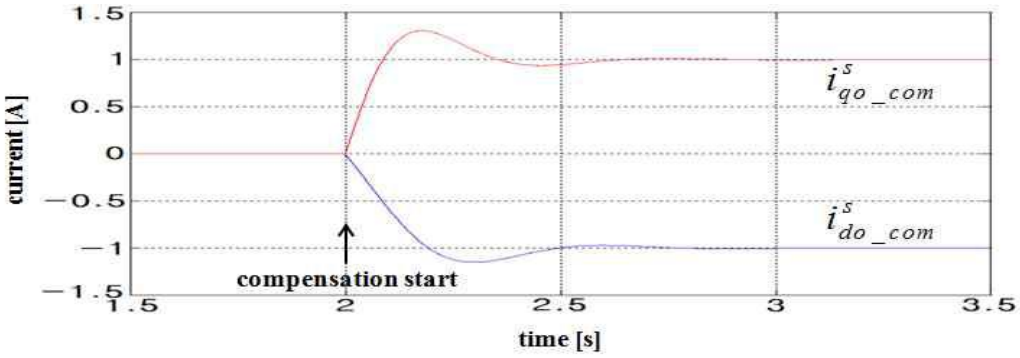

Fig. 10: Output of the current offset compensator in three-phase grid-connected inverters

Conclusion:

These single and three phase current control measurement grid inverter is used as the grid interface of a higher power rated conversion system, since it has only a single and three phase dc source. The proposed fixed current control leads to an equal and uniform distribution of the switching stress among the various switches. It is shown that following the proposed gain calculation method ensures the operation of the circuits which is fixed frequency of the carrier. With the multicarrier level shifted current control, the net switching frequency increases and the ripple magnitude is reduced leading to a higher feed forward gain and hence better control characteristics. It is shown through simulation results that the available measurement can be controlled to feed the load real power with the balance real power being supplied from the grid. In addition to real power injection, the objective of load compensation is also achieved leading to a balanced, distortion free, and unity power factor source current. The voltages across the operation are balanced under all conditions with the proposed control method.

REFERENCES

Carrasco, J.M., L.G. Franquelo, J.T. Bialasiewicz, E. Galvan, R.C.P. Guisado, Mz.A.M. Prats, J.I. Leon, and N. Moreno-Alfonso, 2006. "Power-Electronic systems for the grid integration of renewable energy sources: A survey," *IEEE Trans. Ind. Electron.*, 53(4): 1002-1016.

Min, B.D., J.P. Lee, J.H. Kim, T.J. Kim, D.W. Yoo, K.R. Ryu, J.J. Kim, and E.H. Song, 2008. "A novel grid-connected PV PCS with new high efficiency converter," *Journal of Power Electronics*, 8(4): 309 316.

Jeong, K., B.M. J.Y. Han, Lee and N.S. Choi, 2011. "High-efficiency grid-tied power conditioning system for fuel cell power generation," *Journal of Power Electronics*, 11(4): 551-560.

Kirubakaran, K., S. Jain and R.K. Nema, 2011. "DSP-controlled power electronic interface for fuel-cell-based distributed generation," *IEEE Trans. Power Electron.*, 26(12): 3853-3864.

Singh, B., K. Al-Haddad and A. Chandra, 1999. "A review of active filters for power quality improvement," *IEEE Trans. Ind. Electron.*, 46(5): 960-971.

Mohamed Adel, Sherif Zaid and Osama Mahgoub, 2011. "Improved active power filter performance based on an indirect current control technique," *Journal of Power Electronics*, 11(6): 931-937.

Kwan, K.H., P.L. So and Y.C. Chu, 2012. "An output regulation-based unified power quality conditioner with Kalman filters," *IEEE Trans. Ind. Electron.*, Nov. IEEE Standard for Interconnecting Distributed Resources with Electric Power Systems, IEEE Standard 1547-2003, 59(11): 4248-4262.

Infield, D.G., P. Onions, A.D. Simmons and G.A. Smith, 2004. "Power quality from multiple grid-connected single-phase inverters," *IEEE Trans. Power Del.*, 19(4): 1983-1989.

Gertmar, L., P. Karlsson and O. Samuelsson, 2005. "On DC injection to AC grids from distributed generation," in *Proc. Eur. Conf. Power Electron. Appl.*, pp: 10.

Kazmierkowski, M.P. and L. Malesani, 1998. "Current control techniques for three-phase voltage-source PWM converters: a survey," *IEEE Trans. Ind. Electron.*, 45(5): 691-703.

Kim, R.Y., S.Y. Choi and I.Y. Suh, 2004. "Instantaneous control of average power for grid tie inverter using single phase D-Q rotating frame with all pass filter," in *Proc. IEEE 30th Annu. IEEE IECON*, 1: 274-279.

Zmood, D.N., D.G. Holmes and G.H. Bode, 2001. "Frequency-domain analysis of three-phase linear current regulators," *IEEE Trans. Ind. Appl.*, 37(2): 601-610.

Zmood, D.N. and D.G. Holmes, 2003. "Stationary frame current regulation of PWM inverters with zero steady-state error," *IEEE Trans. Power Electron.*, 18(3): 814-822.

Teodorescu, R., F. Blaabjerg, M. Liserre and P.C. Loh, 2006. "Proportional-resonant controllers and filters for grid-connected voltage-source converters," *IEE Proc.-Electr. Power Appl.*, 153(5): 750-762.

Jiang, S., D. Cao, Y. Li and F.Z. Peng, 2012. "Grid-connected boost-half-bridge photovoltaic microinverter system using repetitive current control and maximum power point tracking," *IEEE Trans. Power Electron.*, 27(11): 4711-4722.

Hang, L., S. Liu, G. Yan, B. Qu and Z. Lu, 2011. "An improved deadbeat scheme with fuzzy controller for the grid-side three-phase PWM boost rectifier," *IEEE Trans. Power Electron.*, 26(4): 1184-1191.

Suul, J.A., K. Ljokelsoy, T. Midtsund and T. Undeland, 2011. "Synchronous reference frame hysteresis current control for grid converter applications," *IEEE Trans. Ind. Appl.*, 47(5): 2183-2194.